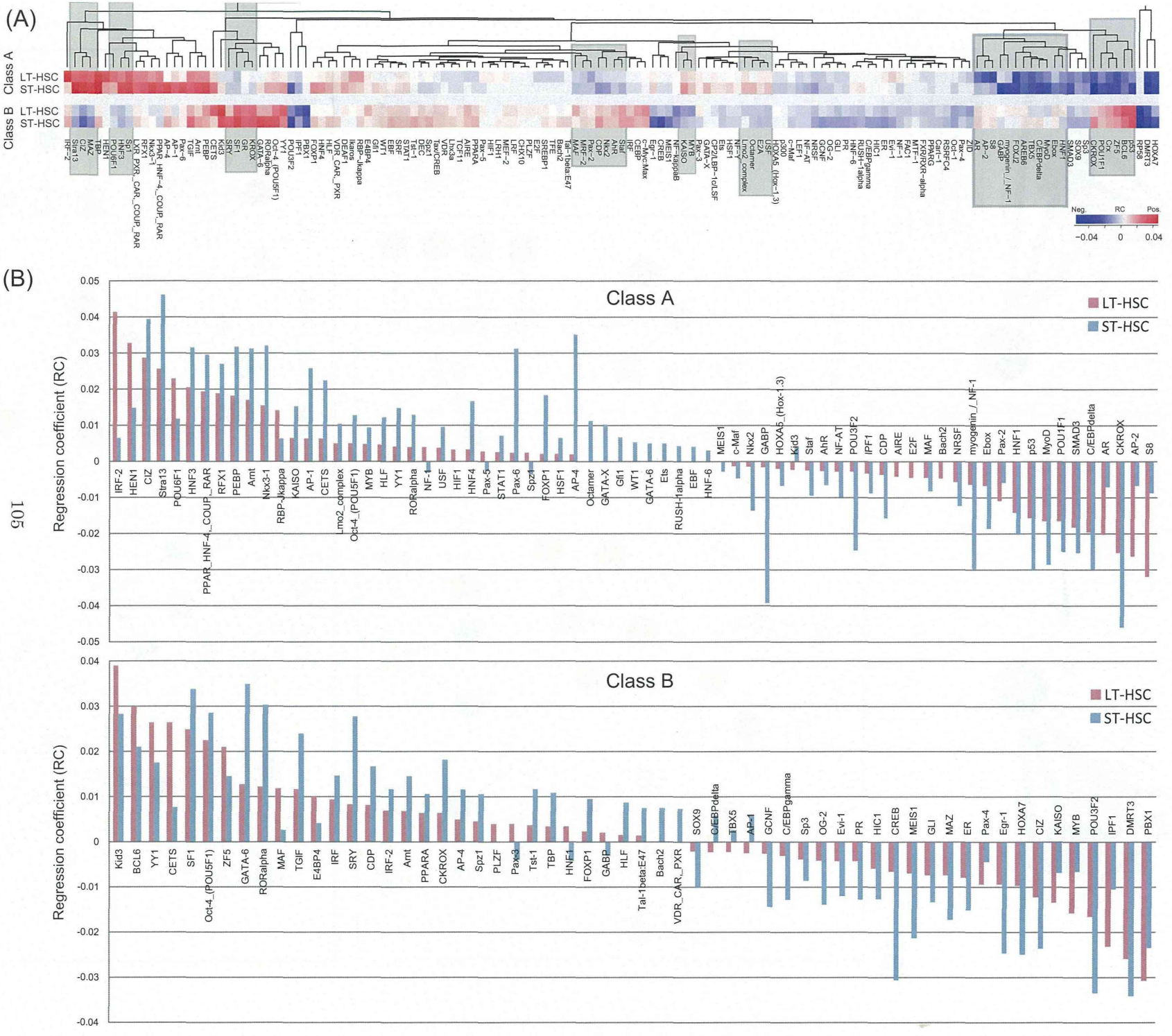
(A)
Class A
LT-HSC
ST-HSC
Class B
LT-HSC
ST-HSC
Neg.
RC
Pos.
−0.04
0
0.04
(B)
Class A
LT-HSC
ST-HSC
Regression coefficient (RC)
0.05
0.04
0.03
0.02
0.01
0
-0.01
-0.02
-0.03
-0.04
-0.05
IRF-2
HEN1
CIZ
Stra13
POU6F1
HNF3
PPAR_HNF-4_COUP_RAR
RFX1
PEBP
Amt
Nkx3-1
RBP-Jkappa
KAISO
AP-1
CETS
Lmo2_complex
Oct-4_(POU5F1)
MYB
HLF
YY1
RORalpha
NF-1
USF
HIF1
HNF4
Pax-5
STAT1
Pax-6
Spz1
FOXP1
HSF1
AP-4
Octamer
GATA-X
Gfi1
WT1
GATA-6
Ets
RUSH1alpha
EBF
HNF-6
MEIS1
c-Maf
Nkx2
GABP
HOXA5_(Hox-1.3)
Kid3
Staf
AhR
NF-AT
POU3F2
IPF1
CDP
AIRE
E2F
MAF
Bach2
NRSF
myogenin_/_NF-1
Ebox
Pax-2
HNF1
p53
MyoD
POU1F1
SMAD3
C/EBPdelta
AR
CKROX
AP-2
S8
Class B
LT-HSC
ST-HSC
Regression coefficient (RC)
0.04
0.03
0.02
0.01
0
-0.01
-0.02
-0.03
-0.04
Kid3
BCL6
YY1
CETS
SF1
Oct-4_(POU5F1)
ZF5
GATA-6
RORalpha
MAF
TGIF
E4BP4
IRF
SRY
CDP
IRF-2
Amt
PPARA
CKROX
AP-4
Spz1
PLZF
Pax3
Tst-1
TBP
HNF1
FOXP1
GABP
HLF
Tal-1beta:E47
Bach2
VDR_CAR_PXR
SOX9
C/EBPdelta
TBX5
AP-1
GCNF
C/EBPgamma
Sp3
OG-2
Evi-1
PR
HIC1
CREB
MEIS1
GLI
MAZ
ER
Pax-4
Egr-1
HOXA7
CIZ
KAISO
MYB
POU3F2
IPF1
DMRT3
PBX1

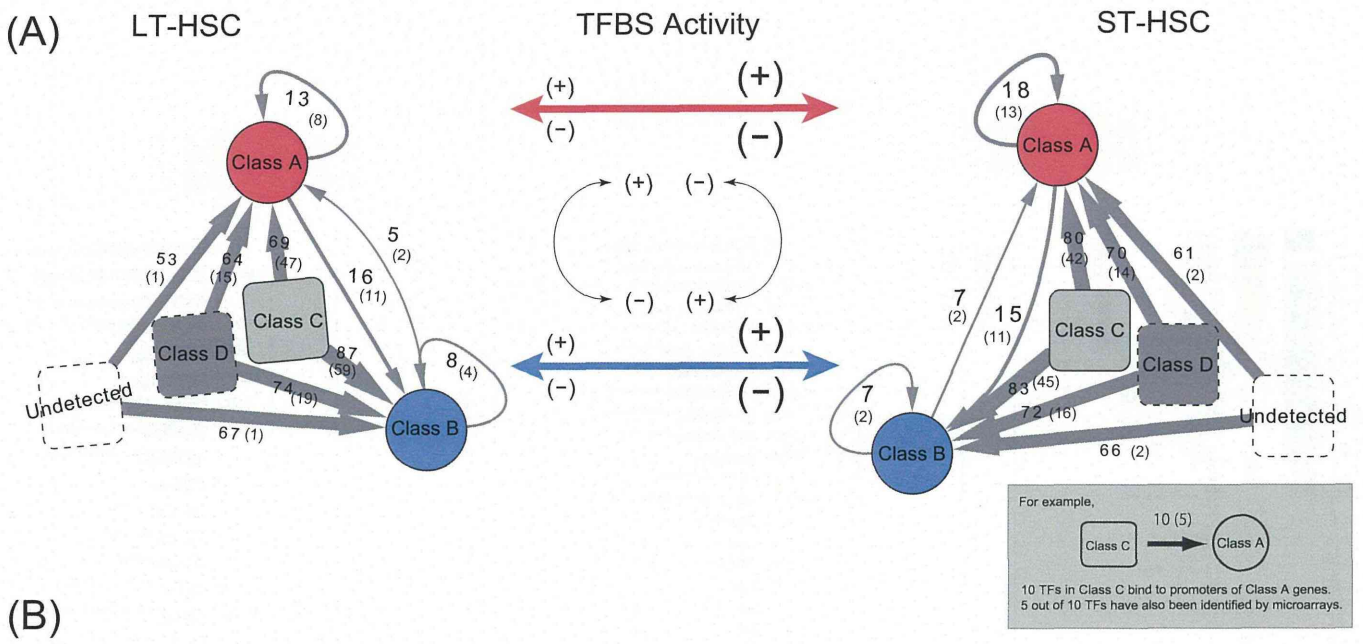
(A)
LT-HSC
TFBS Activity
ST-HSC
Class A
Class B
Class C
Class D
Undetected
13 (8)
5 (2)
53 (1)
64 (15)
69 (47)
16 (11)
87 (59)
8 (4)
74 (19)
67 (1)
18 (13)
80 (42)
70 (14)
61 (2)
7 (2)
15 (11)
83 (45)
72 (16)
66 (2)
For example,
10 (5)
10 TFs in Class C bind to promoters of Class A genes.
5 out of 10 TFs have also been identified by microarrays.

(B)

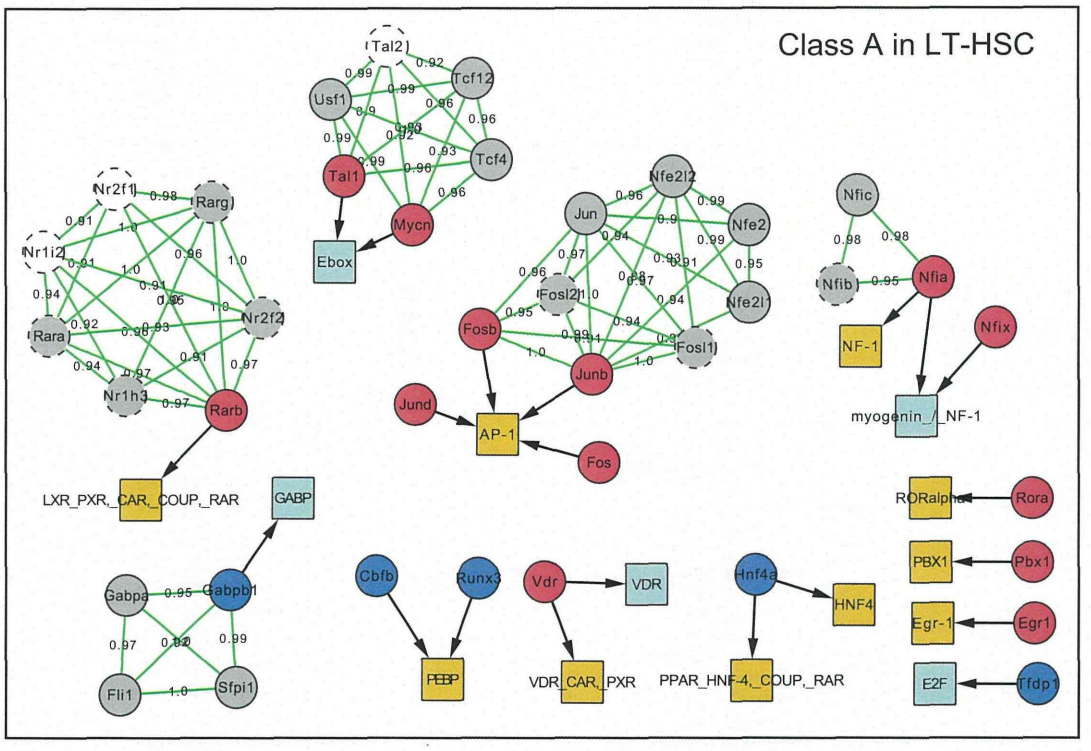
Class A in LT-HSC
Tal2
Tcf12
Usf1
Tcf4
Tal1
Mycn
Ebox
Nr2f1
Rarg
Nr1i2
Rara
Nr2f2
Nr1h3
Rarb
LXR_PXR,_CAR,_COUP,_RAR
GABP
Gabpa
Gabpb1
Fli1
Sfpi1
Nfe2l2
Jun
Nfe2
Fosl2
Fosb
Fosl1
Junb
Jund
AP-1
Fos
Nfic
Nfib
Nfia
NF-1
Nfix
myogenin_/_NF-1
Cbfb
Runx3
PEBP
Vdr
VDR
VDR_CAR_PXR
Hnf4a
HNF4
PPAR_HNF4_COUP_RAR
RORalpha
Rora
PBX1
Pbx1
Egr-1
Egr1
E2F
Tfdp1
TFBS
positive
negative
binding
TF
Class A
Class B
interaction
Class C
Class D
undetected

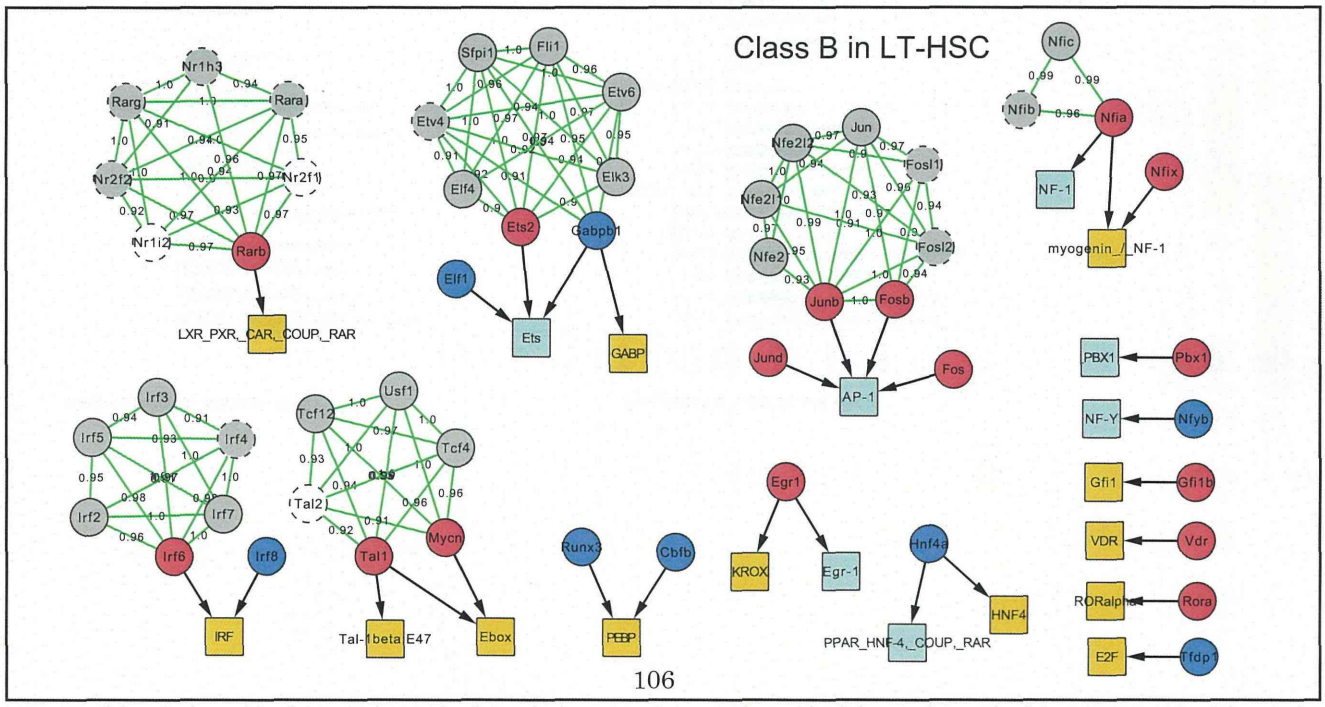
Class B in LT-HSC
Nr1h3
Rarg
Rara
Nr2f2
Nr2f1
Nr1i2
Rarb
LXR_PXR_CAR_COUP_RAR
Sfpi1
Fli1
Etv6
Etv4
Elk3
Elf4
Ets2
Gabpb1
Elf1
Ets
GABP
Nfic
Nfib
Nfia
NF-1
Nfix
myogenin_/_NF-1
Nfe2l2
Jun
Fosl1
Nfe2
Fosl2
Junb
Fosb
Jund
AP-1
Fos
Irf3
Irf5
Irf4
Irf2
Irf7
Irf6
Irf8
IRF
Tcf12
Usf1
Tcf4
Tal2
Tal1
Mycn
Tal-1beta E47
Ebox
Runx3
Cbfb
PEBP
Egr1
KROX
Egr-1
Hnf4a
HNF4
PPAR_HNF4_COUP_RAR
PBX1
Pbx1
NF-Y
Nfyb
Gfi1
Gfi1b
VDR
Vdr
RORalpha
Rora
E2F
Tfdp1

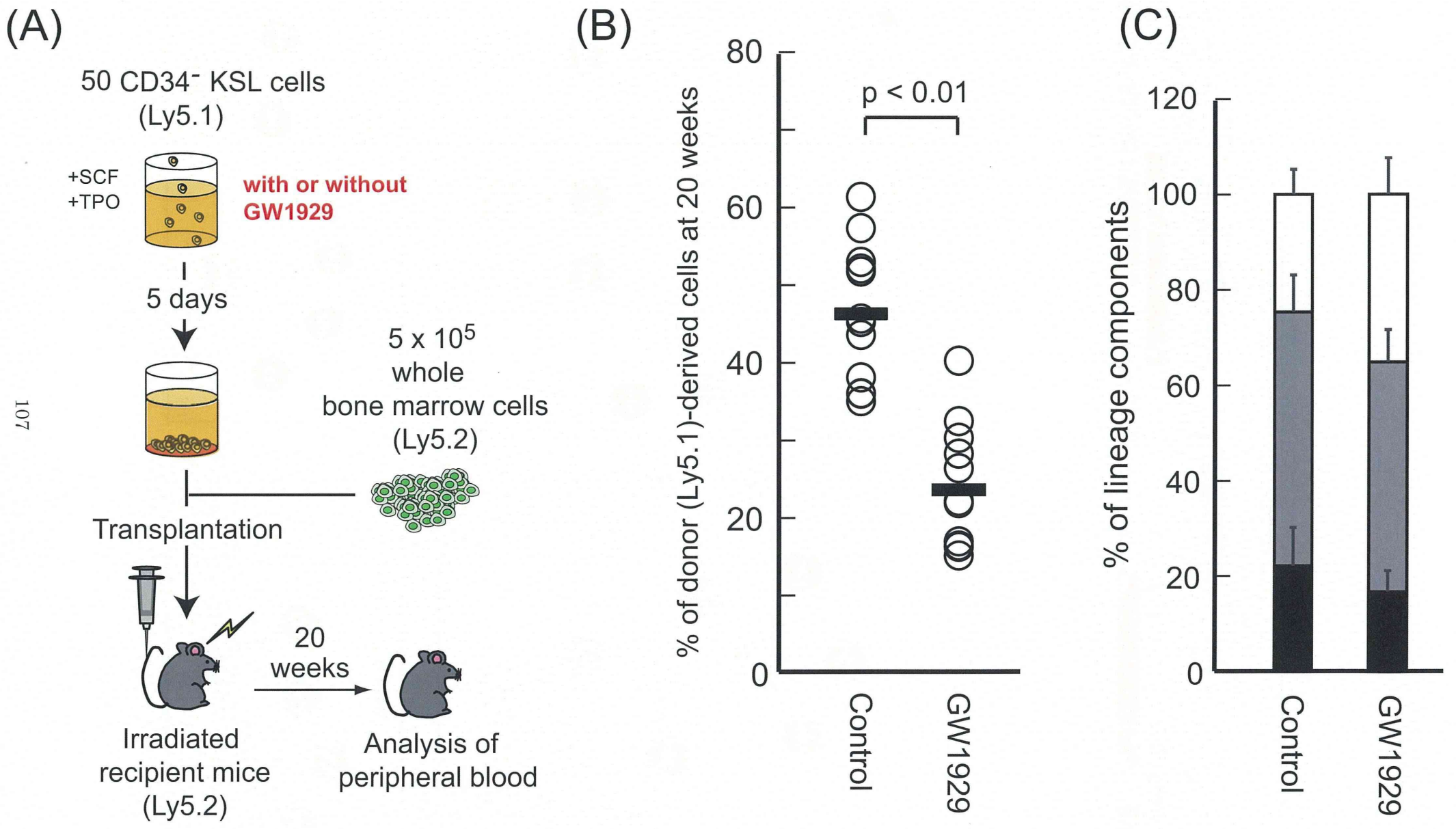
(A)
50 CD34⁻ KSL cells
(Ly5.1)
+SCF
+TPO
with or without
GW1929
5 days
5 x 10⁵
whole
bone marrow cells
(Ly5.2)
Transplantation
20
weeks
Irradiated
recipient mice
(Ly5.2)
Analysis of
peripheral blood
(B)
% of donor (Ly5.1)-derived cells at 20 weeks
80
60
40
20
0
p < 0.01
Control
GW1929
(C)
% of lineage components
120
100
80
60
40
20
0
Control
GW1929

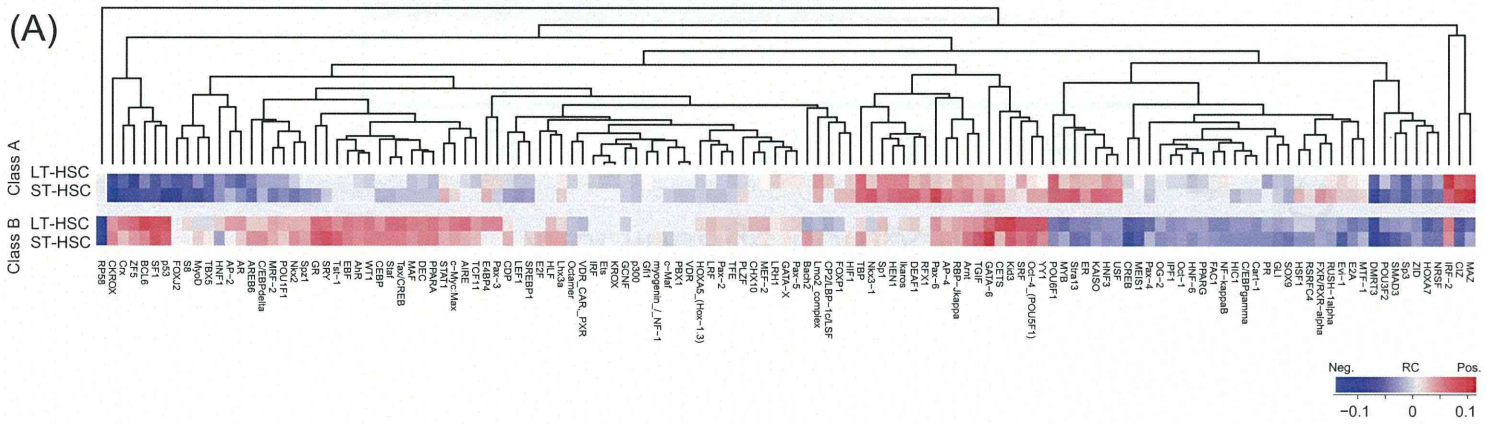
(A)
Class A
LT-HSC
ST-HSC
Class B
LT-HSC
ST-HSC
Neg.
RC
Pos.
−0.1
0
0.1

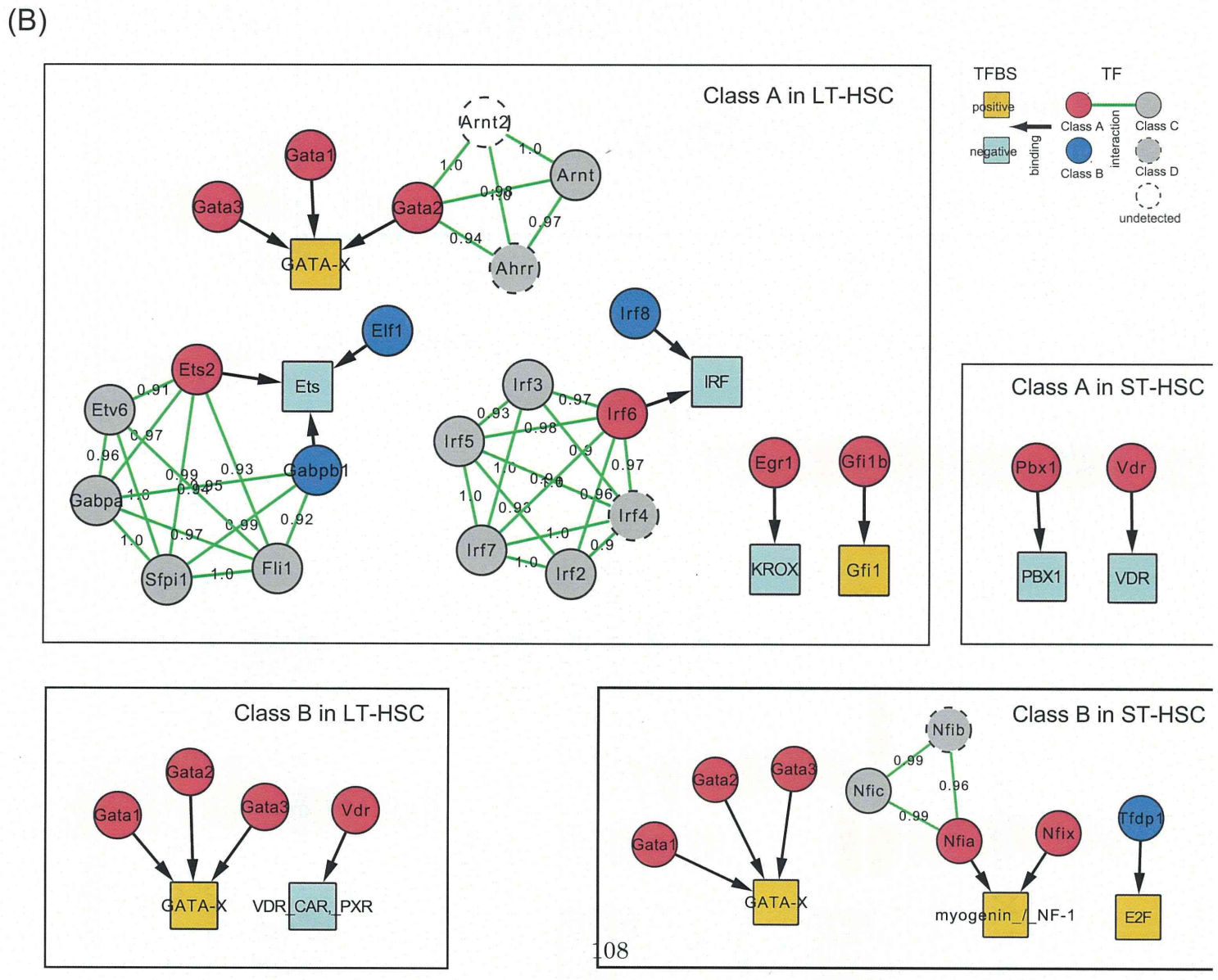
(B)
Class A in LT-HSC
Arnt2
Gata1
Gata3
Gata2
Arnt
Ahrr
GATA-X
Elf1
Ets2
Ets
Etv6
Gabpb1
Gabpa
Sfpi1
Fli1
Irf8
IRF
Irf3
Irf6
Irf5
Irf4
Irf7
Irf2
Egr1
Gfi1b
KROX
Gfi1
TFBS
TF
positive
negative
binding
Class A
Class B
interaction
Class C
Class D
undetected
Class A in ST-HSC
Pbx1
Vdr
PBX1
VDR
Class B in LT-HSC
Gata1
Gata2
Gata3
Vdr
GATA-X
VDR_CAR_PXR
Class B in ST-HSC
Nfib
Gata1
Gata2
Gata3
Nfic
Nfia
Nfix
Tfdp1
GATA-X
myogenin_/_NF-1
E2F

STEM CELLS®

TISSUE-SPECIFIC STEM CELLS

Mesenchymal Stem Cells Cancel Azoxymethane-induced Tumor Initiation

Masanao Nasuno[1], Yoshiaki Arimura[1], Kanna Nagaishi[2], Hiroyuki Isshiki[1], Kei Onodera[1], Suguru Nakagaki[1], Shuhei Watanabe[1], Masashi Idogawa[3], Kentaro Yamashita[1], Yasuyoshi Naishiro[4], Yasushi Adachi[1], Hiromu Suzuki[5], Mineko Fujimiya[3], Kohzoh Imai[6] and Yasuhisa Shinomura[1]

[1]Department of Gastroenterology, Rheumatology, and Clinical Immunology. [2]Department of Anatomy, [3]Department of Medical Genome Sciences, Research Institute for Frontier Medicine, [4]Department of Educational Development, and [5]Department of Molecular Biology, Sapporo Medical University, Chuo-ku, Sapporo 060-8543, Japan, [6]Center for Antibody and Vaccine Therapy, Institute of Medical Science, The University of Tokyo, Tokyo, Japan

Key Words. mesenchymal stem cells • azoxymethane • tumor initiation • colorectal cancer • chemoprevention

ABSTRACT

The role of mesenchymal stem cells (MSCs) in tumorigenesis remains controversial. Therefore, our goal was to determine whether exogenous MSCs possess intrinsic antineoplastic or proneoplastic properties in azoxymethane (AOM)-induced carcinogenesis. Three *in vivo* models were studied: an AOM/dextran sulfate sodium colitis-associated carcinoma model, an aberrant crypt foci model, and a model to assess the acute apoptotic response of a genotoxic carcinogen (AARGC). We also performed *in vitro* coculture experiments. As a result, we found that MSCs partially canceled AOM-induced tumor initiation but not tumor promotion. Moreover, MSCs inhibited the AARGC in colonic epithelial cells because of the removal of O^6-methylguanine adducts through O^6-methylguanine-DNA methyltransferase

Author contributions: M.N.: acquisition, analysis, and interpretation of data; Y.A.: study concept and design, analysis and interpretation of data, drafting of the manuscript, and statistical analysis, K.N.: study concept and design, acquisition, analysis, and interpretation of data, and material support; H.I.: critical revision of the manuscript for important intellectual content and analysis and interpretation of data; K.O.: acquisition, analysis, and interpretation of data; S.N.: acquisition, analysis, and interpretation of data; S.W.: acquisition, analysis, and interpretation of data; M.I.: critical revision of the manuscript for important intellectual content and analysis and interpretation of data; K.Y.: critical revision of the manuscript for important intellectual content and analysis and interpretation of data; H.S.: acquisition, analysis, and interpretation of data; Y.N.: analysis and interpretation of data and critical revision of the manuscript for important intellectual content; Y.A.: critical revision of the manuscript for important intellectual content and analysis and interpretation of data; M.F.: technical and material support, and study supervision; K.I.: obtained funding and administrative support; Y.S.: study supervision and critical revision of the manuscript for important intellectual content.

Correspondence: Yoshiaki Arimura, First Department of Internal Medicine, Sapporo Medical University, S-1, W-16, Chuo-ku, Sapporo 060-8543, Japan., Phone: +81-11-611-2111 (Ext. 3211, 3213), Fax: +81-11-611-2282, E-mail: arimura@sapmed.ac.jp; Grant Support: This study was supported in part by Health and Labour Sciences Research Grants for research on intractable diseases from the Ministry of Health, Labour and Welfare of Japan (K.I.).; Received August 08, 2013; accepted for publication October 12, 2013; 1066-5099/2013/$30.00/0 doi: 10.1002/stem.1594

This article has been accepted for publication and undergone full peer review but has not been through the copyediting, typesetting, pagination and proofreading process which may lead to differences between this version and the Version of Record. Please cite this article as doi: 10.1002/stem.1594

activation. Furthermore, MSCs broadly affected the cell-cycle machinery, potentially leading to G1 arrest *in vivo*. Coculture of IEC-6 rat intestinal cells with MSCs not only arrested the cell cycle at the G1 phase, but also induced apoptosis. The anti-carcinogenetic properties of MSCs *in vitro* required transforming growth factor (TGF)-β signaling because such properties were completely abrogated by absorption of TGF-β under indirect coculture conditions. MSCs inhibited AOM-induced tumor initiation by preventing the initiating cells from sustaining DNA insults and subsequently inducing G1 arrest in the initiated cells that escaped from the AARGC. Furthermore, tumor initiation perturbed by MSCs might potentially dysregulate WNT and TGF-β-Smad signaling pathways in subsequent tumorigenesis. Obtaining a better understanding of MSC functions in colon carcinogenesis is essential before commencing the broader clinical application of promising MSC-based therapies for cancer-prone patients with inflammatory bowel disease.

INTRODUCTION

Stem and progenitor cells are well-known direct cellular targets of genetic alterations in human carcinogenesis [1-3]. Previous studies have altered our perception of stromal cells from being innocent bystanders to active promoters in the neoplastic process [4-6]. Carcinoma formation accompanied by well-orchestrated desmoplastic reactions [7] closely resembles wound healing and scar formation, and entails the constant availability of growth factors, cytokines, and matrix-remodeling proteins that render the tumor site as a 'wound that never heals' [8]. Recent studies have shown that bone marrow-derived mesenchymal stem cells (MSCs) are recruited in large numbers to the stroma of developing tumors [9, 10].

However, the role of MSCs in tumorigenesis remains an intensely debated topic. Khakoo et al. demonstrated that intravenously injected human MSCs possess intrinsic antineoplastic properties in an *in vivo* model of Kaposi's sarcoma by inhibition of Akt activity in a cell-cell contact-dependent manner [11]. In contrast, Karnoub et al. demonstrated that MSCs within the stroma of the tumor microenvironment facilitate metastatic spread via paracrine signals of C-C motif chemokine 5 that is secreted *de novo* by MSCs [12].

A meta-analysis of chemoprevention studies has suggested that azoxymethane (AOM)-based rodent models of carcinogenesis are valuable for prediction of chemopreventive efficacy in humans, which is better than that of other models [13, 14]. The prominent advantages of the AOM/dextran sulfate sodium (DSS) colitis-associated carcinogenesis model are that factors influencing tumor initiation [15, 16] should result in changes of the average tumor number per animal, whereas differences of the average tumor size typically provide evidence for factors involved in tumor progression [17, 18]. AOM is a genotoxic agent that initiates cancer by alkylation of DNA, in which O6-methylguanine (O^6MeG) is a highly cytotoxic, apoptotic, mutagenic, recombinogenic, and clastogenic DNA adduct [19]. Conversely, DSS is not genotoxic, but

rather a proinflammatory tumor promoter [20]. Studies in rodents have revealed that AOM-induced tumors resemble human colorectal cancer at the molecular level, which displays dysregulation of the canonical WNT signaling pathway, similar target genes (21–24), and mutation of *K-ras* [25].

Our goal was to determine whether MSCs possess intrinsic antineoplastic or proneoplastic properties in an AOM-induced tumorigenesis model. Because MSCs are prime candidates for use in cell- and gene-based therapies [26, 27], this essential information must be obtained before implementing the broader clinical application of MSC therapies.

MATERIALS AND METHODS

For detailed Materials and Methods, please refer to Supplementary Data.

Experimental animals

Animal studies were performed under the supervision of the Committee for Animal Research of Sapporo Medical University in accordance with protocols approved by the Institutional Animal Care and Use Committee. All animals were maintained according to the guidelines of the Committee for Animal Research of Sapporo Medical University. Lewis rats were purchased from Charles River Laboratories Japan (Yokohama, Japan) and SD-TG (CAG-EGFP) rats were purchased from Japan SLC, Inc. (Hamamatsu, Japan) [28]. All rats were aged 6 weeks and female unless indicated otherwise and were housed under pathogen-free conditions and received autoclaved food and water ad libitum.

Cell lines and culture conditions

Bone marrow cells were harvested by inserting a needle into the shaft of the femur or tibia and flushing it with 30 mL α-modified Eagle's medium (αMEM) containing 20% fetal bovine serum (FBS). To harvest rat MSCs [29], the cell suspensions were passed through a 70-μm nylon filter (Becton Dickinson, Franklin Lakes, NJ, USA) and plated in 75-cm^2 flasks. Cells were grown in αMEM containing 20% FBS at 37°C and 5% CO_2. After 3 days, the medium was replaced with fresh αMEM containing 10% FBS, and the adherent cells were grown to 80% confluence to obtain passage 0. In accordance with the International Society for Cellular Therapy criteria [30], cells between passages 3 and 5 were used for subsequent experiments [26]. To harvest rat hematopoietic stem cells (HSCs) [31], CD90.1 $(Thy1.1)^+$ cells were magnetically labeled with CD90.1 MicroBeads (Miltenyi Biotec GmbH, Gladbach, Germany) for 15 min. Then, the cell suspension was loaded onto a MACS® column that was placed in the magnetic field of a MACS® separator. The magnetically labeled $CD90.1^+$ cells were retained and then eluted as the positively selected cell fraction. Detailed protocols and data sheets are available at www.miltenyibiotec.com. To prepare conditioned medium from rat MSCs (MSC-CM), MSCs (4×10^5 cells/150-mm culture dish) were seeded and cultured to confluency. Then, the medium was changed to serum-free Dulbecco's modified Eagle's medium (Invitrogen, Carlsbad, CA, USA), and the rat MSCs were cultured for a further 48 h. The conditioned medium was collected, centrifuged at 300 ×*g* for 5 min, filtered using a

0.22-μm syringe filter, and then stored at –80°C until use.

IEC-6 cells obtained from the American Type Culture Collection (Manassas, VA, USA) and 3Y1 rat fibroblasts (3Y1-B Clone 1-6) [32] obtained from JCRB Cell Bank were maintained as recommended by the depositors.

AOM/DSS colitis-associated carcinoma model and evaluation of tumor growth

We adopted the two-stage colon tumor model that mimics colitis-driven tumor development as described by Tanaka *et al.* [33]. Thirty-nine female Lew rats were divided into three groups (n = 13 each group): two treatment groups and one control group (Fig. 1). The control group designated as 'MSC (-)' was administered a single intraperitoneal injection of AOM (15 mg/kg body weight; Sigma-Aldrich, St. Louis, MO, USA) and was not treated with MSCs. Starting at 1 week after injection, the animals received 2.5% DSS (MW 9,000–20,000; Sigma-Aldrich) in drinking water for 7 days, and then received no further treatment for 18 weeks. The group designated as 'MSC Day0' was intravenously administered 2×10^4 MSCs/g body weight on Day 0 when AOM was injected, and the group designated as 'MSC Day9' was administered MSCs on Day 9 following the AOM administration corresponding to Day 2 after receiving DSS in drinking water. Evaluation of tumor growth in the AOM/DSS colitis-associated carcinoma model is described in Supplementary Data.

Analysis of aberrant crypts (ACs)

Fifteen female Lew rats were divided into three groups (n = 5 each group): two treatment groups and one control group (Fig. 3). The control group designated as 'MSC (-)' was administered two separate intraperitoneal injections of AOM (15 mg/kg body weight) at 7 days apart (Days 0 and 7) and was not treated with MSCs. No further treatment was performed for 3 weeks. The group designated as 'MSC Day–1' was intravenously administered 2×10^4 MSCs/g body weight on Day 1, which was 1 day before AOM was first injected, and the group designated as 'MSC Day8' was administered MSCs on Day 8 (1 day after the second AOM administration). The rats were sacrificed at the end of the study (Week 4) by transcardial perfusion with 4% paraformaldehyde in PBS. The colon was removed and cut open from the anus to the cecum along the longitudinal axis. We defined the rectum as the segment at 2 cm proximal to the anus, and divided the entire colon into three segments each measuring approximately 7 cm in length: the distal colon including the rectum and the middle and proximal colon. The colon was spread flat between sheets of filter paper and fixed in 10% buffered formalin. Then, the colon tissues were stained with 0.2% methylene blue in saline according to the procedure described by Bird [34] to observe ACs. Based on the McLellan and Bird [35] definition, ACs were defined as those that (i) were larger than normal crypts, (ii) had an increased pericryptal space that separated them from normal crypts, (iii) had a thicker layer of epithelial cells that often stained darkly, and (iv) generally had oval rather than circular openings. The number of aberrant crypt foci (ACF) per colon, the number of ACs in each focus, and the location of each focus were determined by stereomicroscopy (Olympus, Tokyo, Japan) at ×40 magnification.

The mucosa of the distal segments was scraped off and subjected to western blot analysis.

Effects of MSCs on the acute apoptotic response to a genotoxic carcinogen (AARGC)

The five experimental groups included the MSC-untreated control group administered PBS, the group designated as 'MSC' administered MSCs, groups designated as 'HSC' and '3Y1' administered HSCs or 3Y1 rat fibroblasts, respectively, and the group designated as 'MSC-CM' treated with MSC-CM at 24 h prior to AOM administration. Each group consisted of five rats and received a single subcutaneous injection of AOM (15 mg/kg body weight) at 09:00 h. The rats were then sacrificed by CO_2-induced narcosis at the indicated intervals from 8 to 48 h. The entire colon was removed immediately, cut open, and flushed with ice-cold saline. Segments measuring 2 cm were taken from the rectal end of the distal portion. These segments were immediately fixed in 10% paraformaldehyde overnight at room temperature and then embedded in paraffin. The mucosa on the remaining segments was scraped off and subjected to subsequent analyses.

β-catenin nucleotide sequence

Sequencing was performed by the classical Sanger method [36].

WNT signaling pathway PCR array analysis

A Rat WNT Signaling Pathway RT^2 Profiler™ PCR Array (SuperArray Bioscience, Frederick, MD, USA) was performed according to the manufacturer's instructions.

Analysis of the cell cycle and apoptosis

The cell cycle was assessed by flow cytometry and Ki67 immunohistochemistry. The apoptotic cell fraction was determined by terminal deoxynucleotidyl transferase-mediated dUTP nick-end labeling (TUNEL) reactions.

Immunofluorescence of the DNA adduct of O^6MeG

The level of DNA alkylation was analyzed by immunofluorescence of distal colon sections using an antibody specific for the DNA adduct of O^6MeG. Frozen sections (4 μm) were prepared, rehydrated, and incubated with 3% H_2O_2 in 50% ethanol for 15 min at room temperature. Antigen retrieval was carried out with a Retrieval Solution (DAKO, Carpinteria, CA, USA) for 10 min at 105°C in an autoclave. RNase treatment (20 μL RNase A at 10 mg/mL and 5 μL RNase T at 10 U/mL in 1,000 μL PBS, pH 7.5) was carried out for 1 h at 37°C, and then stopped by treatment with a 140 mmol/L NaCl solution for 5 min at 4°C. DNA unwinding was achieved by alkali treatment (1,500 μL of 70 mmol/L NaOH/140 mmol/L NaCl and 1,000 μL of absolute methanol) before applying Protein Block (DAKO) for 10 min at room temperature. The sections were then incubated at room temperature overnight with an anti-O^6MeG monoclonal antibody (clone EM 2-3; Squarix Biotechnology, Marl, Germany) diluted at 1:1,000 in PBS. The next day, the sections were washed in PBS three times for 5 min each before applying an Alexa Fluor® 594-labeled secondary anti-mouse IgG. Sections were counterstained with DAPI, dehydrated, and cover slipped for observation under a LSM 510 META. The primary antibody was omitted for the negative control.

MTT assay

Cell proliferation was measured by a MTT dye reduction assay [37].

RNA isolation and quantitative real-time PCR (qPCR) analysis

qPCR was performed using TaqMan® Universal PCR Master Mix (Applied Biosystems) for 40 cycles at 95°C for 15 s and 60°C for 1 min by standard methods.

Western blot analysis

Western blot analysis was performed according to standard methods.

MSC and IEC-6 cell coculture experiments

Green fluorescent protein (GFP)-labeled rat MSCs were cocultured with the rat small intestinal cell line IEC-6. MSCs and IEC-6 cells cultured separately were included as controls. The cells were cocultured in RPMI 1640 (Sigma-Aldrich) supplemented with 10% FBS, penicillin (100 U/mL), and streptomycin (100 μg/mL) at 37°C with 5% CO_2. A total of 1×10^6 MSCs were seeded per 100-mm dish for the MSC control and harvesting MSC-CM, and 1×10^6 IEC-6 cells per dish for the cell line control. For direct coculture, 1×10^6 MSCs per dish were preseeded for 2–3 h. Then, 1×10^6 IEC-6 cells per dish were added and cultured for up to 72 h with/without AOM treatment. For indirect coculture, 1,250 IEC-6 cells per well were preseeded in the lower chamber of a Transwell® (0.4-μm pores, 48 wells; Corning, Lowell, MA, USA) for 2–3 h. Then, the same number of MSCs per well were added to the upper chamber of the Transwell® and cultured for up to 72 h with/without AOM, methylazoxymethanol (MAM; Wako Pure Chemical Industries, Tokyo, Japan), or O^6-benzylguanine (O^6BG; Sigma-Aldrich), which binds irreversibly to and inhibits the DNA repair enzyme O^6-methylguanine-DNA methyltransferase (Mgmt). Because AOM is metabolized into the active metabolite MAM by Cyp2e1, we confirmed whether *Cyp2e1* was expressed in IEC-6 cells [38]. For absorption of transforming growth factor (TGF)-β, 1.0 μg/mL anti-TGF-β neutralizing antibody (Clone # 9016; R&D Systems, Minneapolis, MN, USA) was added to the direct coculture condition.

Statistical analysis

To compare means between two groups, parametric and nonparametric analyses were performed using the unpaired Student's *t*-test and the Mann-Whitney U-test, respectively. Categorical variables were compared using the chi-square test, exact *P* value based on Pearson's statistic, or the Monte Carlo method. For multiple comparisons, we applied analysis of variance (ANOVA), especially in serial assessments, and two-way repeated measures (mixed between-within subjects) ANOVA followed by the Bonferroni test [39]. A difference was considered significant at $P < 0.05$ in all two-tailed tests. The SPSS Statistics 17.0 software package (SPSS Inc., Chicago, IL, USA) was used for all statistical analyses.

RESULTS

MSCs reduce the tumor number but not the tumor size in AOM/DSS colitis-associated tumorigenesis

We explored whether MSCs affected tumor initiation or promotion in the AOM/DSS model

and the associated mechanism (Fig. 1A). The average tumor number per rat was significantly decreased by up to half of the expected level when MSCs were simultaneously injected with AOM (MSC Day0 group) ($P = 0.008$ compared with the untreated control and $P = 0.023$ compared with the MSC Day9 group; upper panel in Fig. 1B and Supplementary Fig. S1A). In contrast, the average tumor diameter was not significantly different among the groups as shown in the lower panel of Figure 1B. In this model, factors that influence tumor initiation should result in changes of the average tumor number per animal, whereas differences in average tumor sizes typically provide evidence of factors involved in tumor progression [18]. Therefore, these results suggest that MSC partially cancel AOM/DSS-induced tumor initiation.

MSCs profoundly affect the mutational spectra during the tumor initiation phase

As shown in Figure 1C, the tumor β-catenin expression analyzed by western blotting was not significantly different among MSC (-), MSC Day0, and MSC Day9 groups. However, β-catenin was more frequently phosphorylated (56%, 14/25 tumors) in the MSC Day0 group than that in the MSC (-) group (13.8%, 4/29 tumors) and the MSC Day9 group (12.5%, 2/16, $P = 0.0006$). Furthermore, the mutation spectrum of β-catenin was quite different between MSC (-) and MSC Day0 groups. The codon 34 missense mutation (GGA–GAA) was the most frequent (11/25, 44%) in the MSC (-) group. In addition to the above mutation (5/15, 33.3%), the codon 32 missense mutation (GAT–AAT) was also frequently mutated (5/15, 33.3%) in the MSC Day0 group. Four (66.7%) of the six mutated regions detected in the MSC Day0 group and 12 (85.7%) of the 14 regions detected in the MSC (-) group appeared to be unique (Supplementary Table S3). Seventy-nine (88.8%) of the 89 genes of the WNT signal pathway examined in the WNT PCR array were downregulated in MSC Day0 tumors compared with that in MSC (-) tumors (Fig. 1D).

Receptor-regulated Smad representing canonical TGF-β-Smad signaling was confined to the cell membrane of the laminar propria stromal cells, and β-catenin was expressed only on the cell membranes of crypt epithelial cells in the normal colon (Fig. 2A). Phospho-Smad2 expression representing activated TGF-β signaling was not significantly different between MSC (-) and MSC Day0 groups in western blot analyses (data not shown). The total Smad2 protein level was upregulated locally in the cytoplasm and partially in the nuclei (white arrowheads in Fig. 2B). β-catenin was slightly upregulated in membranous and cytoplasmic staining of the colon carcinomas in MSC (-) group rats (Fig. 2B). In contrast, both Smad2 and β-catenin were localized only on the membrane of colon carcinoma cells in MSC Day0 group rats (Fig. 2C). MSC engraftment was observed in tumors established at 20 weeks after AOM administration (data not shown), Therefore, these results suggest that MSCs profoundly affect the mutational spectra during the tumor initiation phase, leading to distinct WNT and canonical TGF-β-Smad signaling in subsequent tumorigenesis and even in the established tumors.

MSCs reduce the formation of ACF

Next, we determined whether MSCs affect ACF formation and the timing of MSC administration during tumor initiation induced by AOM for the most efficacious chemoprevention (Fig. 3A). The average ACF density was significantly lower in both pre-AOM (MSC Day–1; P = 4.7E-4) and post-AOM (MSC Day8; P = 0.001) treatment groups than that in the MSC (-) control group (Fig. 3B and Supplementary Fig. S1B). As depicted in Figure 3C, ACF were formed more frequently in the distal colon than in the proximal colon as reported previously [34]. ACF formation was suppressed in both the distal and middle colons of both treatment groups (MSC Day–1 and MSC Day8) with no significant differences between the two treatment groups. The multiplicity of ACs per focus, as shown in Figure 3D1 (one AC) to D4 (>four ACs), was reciprocally related to the frequency of the ACs. Among these ACs, one AC/focus was significantly reduced by MSC treatment, although there were no significant difference between the treatment groups (Fig. 3E). Canonical TGF-β-Smad signaling represented by phospho-Smad2 was activated in all colonic epithelia (5/5) of the MSC Day8 group and not in the colonic epithelia of MSC (-) or MSC Day–1 groups (Fig. 3F). Surprisingly, these results suggest that MSCs elicit a chemopreventive effect on formation of the prototype ACF (one AC/focus), both as a preventive measure in the pre-initiation phase (MSC Day–1) and a treatment measure in the post-initiation phase (MSC Day8). However, it is unknown why the canonical TGF-β-Smad signals were distinctly activated by the two measures.

MSCs suppress the AARGC

To obtain a further mechanistic insight into the antineoplastic properties of MSCs in AOM-induced carcinogenesis, we examined whether MSCs affect the AARGC *in vivo* (Fig. 4A) [40]. The AARGC peaked at 8 h after AOM administration, which was significantly suppressed only in the MSC-treated group compared with that in the MSC-untreated control, HSC, 3Y1, and MSC-CM groups (Fig. 4B and 4C). The Ki-67 labeling index of the colonic epithelia was significantly decreased at 24 and 48 h only in the MSC group compared with that in the other groups (Fig. 4D and 4E). Western blot analyses revealed suppression of Akt in the AARGC (8 h) observed in control groups was significantly activated in MSC groups, whereas activation of p38 in the AARGC observed in control groups was slightly suppressed in MSC groups (Fig. 4F). Consequently, these results suggest that AARGC suppression is a specific property of MSCs, which does not involve other cell types or humoral factors produced by MSCs. Because the AARGC is accepted as one of the *in vivo* mechanisms that suppress tumorigenicity, further experiments are necessity to explain why MSCs possess chemopreventive and AARGC suppression effects.

MSCs reduces the amount of DNA adducts of O^6MeG

After administration, AOM is metabolized into MAM by Cyp2e1, which causes a DNA adduct of genotoxic O^6MeG. The methyl moiety in O^6MeG is then enzymatically removed by Mgmt. Therefore, we examined whether MSCs affect the level of O^6MeG using the above model to assess the AARGC *in vivo*. At 8 h after

AOM treatment, massive amounts of O^6MeG adducts were found in the colonic epithelia of MSC (-) control rats by O^6MeG immunofluorescence analysis (Fig. 5A). Furthermore, the amount of O^6MeG adducts was significantly reduced in the MSC-treated group (Fig. 5B). There were almost no positive signals for DNA adducts in healthy rats without AOM treatment at a basal physiological level (Fig. 5C). Moreover, at 8 h after AOM exposure, the amount of *Mgmt* transcripts was more abundant in MSC-treated groups than that in MSC-untreated control groups (Fig. 5D). These results suggest that MSCs indirectly remove O^6MeG adducts, likely though Mgmt activation.

MSCs profoundly affect the cell-cycle machinery

In western blot analyses of the cell-cycle machinery (Fig. 5E), phospho-Smad2 was upregulated at 24 h in the MSC-treated group. Expression of both IκBα and p21 was gradually upregulated in the treated group, whereas it was gradually downregulated in the control group. Accordingly, *p21* expression was upregulated at 4–8 h in the MSC group as revealed by qPCR (data not shown). IKK phosphorylates NFκB bound to IκBα, leading to degradation of IκBα and allowing NF-κB signal activation. p21 Waf1/Cip1 are members of the Cip/Kip family of cyclin-dependent kinase (Cdk) inhibitors, which form heterotrimeric complexes with cyclins and Cdks, inhibiting kinase activity and blocking progression through G1/S phase. Expression of Bax, a pro-apoptotic protein belonging to the Bcl-2 family, was slightly reduced in the treated group. Cyclin Ds induced by mitogenic stimuli form a complex with Cdks. Cyclin D-dependent kinase 4 (Cdk4) complexes, which sequentially phosphorylate the retinoblastoma protein (Rb), facilitate G1–S transition. Cdk4 and phospho-Rb appeared to be downregulated in the treated group. Taken together, MSCs might induce G1 arrest in colon epithelia, even after the AARGC, partially through the canonical TGF-β-Smad signaling pathway.

MSCs induce G1 arrest and/or apoptosis in IEC-6 cells mediated by TGF-β *in vitro*

Intriguingly, MSC suppressed ACF tumorigenesis even in the post-initiation phase (Fig. 3). Furthermore, in the model assessed on the AARGC, MSCs inhibited the cell-cycle machinery of cells evading the AARGC (Fig. 5). These observations strongly suggest that there are additional chemopreventive mechanisms of MSC other than a reduction of mutation load with O^6MeG. To investigation further, we conducted the following coculture experiments under AOM exposure. O^6BG irreversibly inhibits Mgmt that demethylates O^6MeG caused by MAM. Thus, before AOM treatment, we confirmed that *Cyp2e1* was expressed in IEC-6 cells (data not shown) as previously reported [38]. AOM exposure maintained proliferation and suppressed apoptosis of IEC-6 cells without coculture (the first blue bar in Fig. 6A and 6B, and the red line in Fig. 6F). In contrast, IEC-6 cells cocultured with MSCs always showed inhibition of cell proliferation and acceleration of apoptosis depending on the received mutation load. The mutation load corresponded to the level of O^6MeG adduct depending on both the concentration and exposure time of the active metabolite, MAM (Fig. 6A and 6B). AOM

treatment represented a minimal mutation load, whereas MAM plus O^6BG treatment represented the maximal mutation load in this setting. IEC-6 cells cocultured with MSCs under AOM exposure for 72 h exhibited a significant reduction of proliferative activity (the first blue and second red bar in Fig. 6A, 6C, and 6D). Cell-cycle analysis by flow cytometry revealed that IEC-6 cells cocultured under AOM exposure developed G1 arrest after 72 h (Fig. 6E). To obtain a mechanistic insight into these phenomena, MTT assays under AOM exposure were performed using IEC-6 cells, IEC-6 cells treated with MSC-CM, IEC-6 cells directly or indirectly cocultured with MSCs, and IEC-6 cells directly cocultured with MSCs under anti-TGF-β antibody exposure (Fig. 6F). Because the cells in both direct and indirect coculture were able to retain antiproliferative properties, the humoral factors present under a direct heterotypic cell-cell interaction appeared to be important. This property of MSCs was completely abrogated by absorption of TGF-β by neutralizing antibodies.

DISCUSSION

MSCs exhibit chemopreventive properties by primarily canceling AOM-induced tumor initiation

MSC administration led to a dramatic decrease of tumor incidence by up to half of the expected level without affecting the tumor size in the AOM/DSS colitis-associated carcinoma model (Fig. 1B). Consequently, our findings strongly suggest that MSCs exhibit chemopreventive properties by canceling AOM/DSS-induced tumor initiation. ACF, which are putative precursor lesions of colon tumors, represent alternative early end-points in AOM-induced colon carcinogenesis [34, 41, 42]. Although the early form of ACF, namely a single AC per focus, was most frequently observed in our analysis, it was significantly decreased by MSC treatment independent of the timing of AOM administration (Fig. 3). This finding strongly suggests that MSCs do not reduce dysplastic ACF, but rather block ACF formation itself. This result motivated us to analyze the chemopreventive mechanisms exerted by MSCs as early as the AARGC in AOM-induced tumorigenesis.

The AARGC is apparently suppressed by MSC administration

Because evasion of apoptosis is one of the hallmarks of cancer [16], induction of apoptosis during carcinogenesis is a critical step in chemoprevention. It is an accepted notion that the AARGC might regulate the mutational load in the colon or eliminate DNA-damaged cells that might otherwise progress to malignancy [43]. Therefore, most chemopreventive agents enhance the AARGC. Counterintuitively, in this study, the AARGC was seemingly suppressed by up to one-third following MSC treatment in the *in vivo* model compared with that in the MSC-untreated control (Fig. 4C). In contrast to our *in vivo* observations, *in vitro* experiments revealed that MSCs not only inhibited the proliferation of IEC-6 cells in coculture, but also accelerated apoptosis depending on the mutation load of the O^6MeG adduct level (Fig. 6). This discrepancy between *in vitro* and *in vivo* observations concerning apoptosis arises from investigations of the different phases of tumorigenesis between the two observations. MSCs can apparently prevent the AARGC *in*

vivo because of pruning the DNA insults of O^6MeG adducts in the initiating cells, likely through Mgmt activation [44] or because of reducing production of the DNA adduct through Cyp2e1 inhibition [45]. These assumptions are directly supported by the immunofluorescence analysis showing that O^6MeG adducts were significantly decreased by MSC treatment. However, because MSCs upregulated *Mgmt* expression in the colonic mucosa of the AARGC model (Fig. 5A–C), the former pruning mechanism is more likely. In contrast to *in vivo* observations, increasing the mutation load of O^6MeG adducts using a combination of AOM or MAM with O^6BG linearly induced an increase of IEC-6 cell apoptosis *in vitro* (Fig. 6B). Cocultured MSCs directly augmented apoptosis caused by the mutation load of O^6MeG adducts in *vitro*, causing a discrepancy in the results regarding apoptosis between *in vitro* and *in vivo* observations. Our *in vitro* experiments examined the effects of MSCs on the survival of initiated cells beyond the AARGC, which corresponds more to the later phase of tumorigenesis than that in *in vivo* experiments. The detailed underlying mechanisms warrant further analyses.

MSCs induce O^6MeG-triggered G1 arrest and/or apoptosis in the initiated cells evading the AARGC

We determined whether cells that escape from the AARGC subsequently undergo G1 arrest or apoptosis *in vivo*. A reduction of ACF formation was observed by post-AOM treatment of MSCs representing initiated cells entering the post-initiation stage and pre-AOM treatment of MSCs representing cells that remained at the pre-initiation stage (Fig. 3A and 3B). Therefore, additional chemopreventive mechanisms appear to be exerted by MSCs other than a reduction of DNA insults. MSC-IEC-6 coculture experiments revealed that MSCs induced not only G1 arrest in IEC-6 cells, but also enhanced apoptosis depending on the mutational load received by AOM (Fig. 6A and 6B). These antineoplastic and proapoptotic properties of MSCs observed *in vitro* required TGF-β signaling because they were completely abrogated by absorption of TGF-β in cocultures (Fig. 6F). However, in contrast to the *in vitro* study, MSC treatment broadly affected the cell-cycle machinery to facilitate G1 arrest in colon epithelial cells *in vivo* (Fig. 5E). Moreover, it is unlikely that massive apoptosis occurs beyond the AARGC because the apoptotic index was distributed unimodally by steadily increasing and reaching a peak at the AARGC and then steadily decreasing for up to 48–72 h (Fig. 4C). Apoptosis is caused by a series of complex responses involved in mismatch repair machineries and DNA double-strand breaks in subsequent consecutive and replicative cell cycles [46]. Consequently, a longer and closer observation is required to fully determine whether MSCs can induce O^6MeG-triggered apoptosis after evasion of the AARGC *in vivo*. In summary, MSCs reduce the number of initiating cells by pruning O^6MeG and/or inducing G1 arrest through TGF-β signaling in early initiated cells (Fig. 7).

Future challenges for better understanding chemopreventive property of MSC

The mechanism of the first chemopreventive property of MSC, which was attributed to activation of *Mgmt* expression levels by MSCs, remains to be elucidated. MGMT expression is

lost by epigenetic silencing in a variety of human cancers including nearly half of sporadic colorectal cancers [44]. On the other hands, similar to human colorectal cancer, AOM-induced tumors display global DNA hypomethylation. In addition, *Mgmt* is methylated in both AOM tumors and normal colon mucosa [49]. Collectively, these data suggest that epigenetic silencing of *Mgmt* by AOM treatment can be abrogated by MSCs via unknown mechanisms. Thus far, at least three different layers have been elucidated for epigenetic regulation influencing the expression of MGMT: promoter methylation, histone modifications [50], and alternative polyadenylation with consecutive miRNA targeting [51]. Further studies are needed to confirm how MSCs cancel epigenetic silencing of Mgmt and which of the above regulatory mechanisms contribute to this process.

The level of cytosolic β-catenin is controlled by the so-called "β-catenin destruction complex" that facilitates casein kinase 1 alpha (CKIα)- and GSK3 (glycogen synthase kinase)-mediated serial phosphorylation and subsequent polyubiquitination/degradation of β-catenin. However, missense β-catenin mutations at phosphorylation sites are known to prevent β-catenin degradation. In our study, we showed that MSCs facilitated β-catenin phosphorylation in the established tumors of the AOM/DSS model because MSCs induced a unique mutation spectrum of the β-catenin gene during the tumor initiation phase (Figure 1C and Supplementary Table S3). Degradation of Phospho β-catenin is more likely to occur, which can lead to a reduction of Wnt signal activity. In support of this notion, the expression of most WNT signaling pathway molecules appeared to be suppressed in the tumors from MSC Day0 groups as shown by the WNT PCR array analysis (Fig. 1D). However, it largely remains to be clarified how alteration of the mutational spectra leads to a distinct sequela of tumor promotion and progression. The best-defined location of TGF-β/Wnt cross-talk is in the nucleus, where the Smad/β-catenin/Lymphoid enhancer-bind (Lef) protein complex regulates numerous shared target genes, often in a synergistic manner. The implication of cooperative TGF-β and Wnt signaling in tumor progression has recently been examined by Labbé et al. [52]. We demonstrated activation of both canonical pathways of TGF-β and Wnt, whereas both pathways were suppressed by MSCs even in established tumors in which we could not detect any engrafted MSCs. Collectively, these findings suggest that MSCs appear to exert broader and more long-lasting so-called third mechanisms of chemoprevention, which extend beyond the tumor initiation phase in the AOM-induced tumorigenesis via regulation of the cross-talk between canonical Tgf-β and Wnt signaling pathways than discussed heretofore.

Loss of canonical TGF-β-SMAD signaling is considered an essential step in carcinogenesis [53]. In fact, the activity of the Tgf-β pathway is decreased by AOM treatment [54-56]. Tgf-β expression has been found to be reduced in ACF [57, 58] but enhanced in colonic adenomas [57] and adenocarcinomas [59]. These observations suggest dual roles of Tgf-β as an initial tumor suppressor and later as a tumor promoter in AOM-induced carcinogenesis as reported previously [47, 48]. Therefore, MSC activation

of canonical Tgf-β-Smad signaling as a tumor suppressor only in the early initiated cells of the post-AOM MSC treatment group on day 8 in the ACF model (MSC Day8; Fig. 3F) suggests "the second" chemopreventive mechanism of MSCs as discussed in detail earlier. Although canonical Tgf-β-Smad signaling was found to be activated in the established AOM/DSS tumors, Tgf-β signal as a tumor promoter was inhibited in the tumor tissues from the MSC Day0 group (Fig. 2). This alteration of the signal probably reflects the whole integrated signals of a wide array of mutational events and likely does not reflect the effects of MSCs injected in the prior 20 weeks. However, it should be clarified whether this alteration of the Tgf-β signal is related to the above "third" mechanisms of chemoprevention via the cross-talk between the canonical Tgf-β and Wnt signaling pathway.

CONCLUSION

Exogenous MSCs possess intrinsic antineoplastic properties against AOM-induced carcinogenesis. Although a complete mechanistic insight into the properties of MSCs has yet to be achieved, MSCs act as early as tumor initiation events either to reduce the number of initiating cells and/or to induce G1 arrest in early initiated cells (Fig. 7). Obtaining this information is essential before commencing the broader clinical application of promising MSC-based therapies for cancer patients, particularly cancer-prone patients with inflammatory bowel disease.

ACKNOWLEDGMENTS

We are very grateful to Ms. K Fujii at the Department of Gastroenterology, Rheumatology, and Clinical Immunology for providing technical assistance.

Disclosure of potential conflicts of interests

The authors indicate no potential conflicts of interest.

REFERENCES

1. Scadden DT. Cancer stem cells refined. NAT IMMUNOL 2004;5:701–703.
2. Reya T, Morrison SJ, Clarke MF, et al. Stem cells, cancer, and cancer stem cells. NATURE 2001;414:105–111.
3. Sell S. Stem cell origin of cancer and differentiation therapy. CRIT REV ONCOL HEMATOL 2004;51:1–28.
4. Bhowmick NA, Neilson EG, Moses HL. Stromal fibroblasts in cancer initiation and progression. NATURE 2004;432:332–337.
5. Bhowmick NA, Chytil A, Plieth D, et al. TGF-beta signaling in fibroblasts modulates the oncogenic potential of adjacent epithelia. SCIENCE 2004;303:848–851.
6. Orimo A, Gupta PB, Sgroi DC, et al. The influence of the microenvironment on the malignant phenotype. MOL MED TODAY 200;6:324–329.

7. Bissell MJ, Radisky D. Putting tumours in context. NATURE REV CANCER 2001;1:46–54.
8. Dvorak, H. F. Tumors: wounds that do not heal. Similarities between tumor stroma generation and wound healing. N ENGL J MED 1986;315:1650–1659.
9. Hall B, Andreeff M, Marini F. The participation of mesenchymal stem cells in tumor stroma formation and their application as targeted-gene delivery vehicles. HANDB EXP PHARMACOL 2007;180:263–283.
10. Ruan J, Ji J, Song H, et al. Fluorescent magnetic nanoparticle-labeled mesenchymal stem cells for targeted imaging and hyperthermia therapy of in vivo gastric cancer. NANOSCALE RES LETT 2012;7:309.
11. Khakoo AY, Pati S, Anderson SA, et al. Human mesenchymal stem cells exert potent antitumorigenic effects in a model of Kaposi's sarcoma. J EXP MED 2006;203:1235–1247.
12. Karnoub AE, Dash AB, Vo AP, et al. Mesenchymal stem cells within tumour stroma promote breast cancer metastasis. NATURE 2007;449:557–565.
13. Corpet DE, Pierre F. How good are rodent models of carcinogenesis in predicting efficacy in humans? A systematic review and meta-analysis of colon chemoprevention in rats, mice and men. EUR J CANCER 2005;41:1911–1922.
14. Neufert C, Becker C, Neurath MF. An inducible mouse model of colon carcinogenesis for the analysis of sporadic and inflammation-driven tumor progression. NAT PROT 2007;2:1998–2004.
15. Fearon ER, Vogelstein B. A genetic model for colorectal tumorigenesis. CELL 1990;61:759–767.
16. Hanahan D, Weinberg RA. The hallmarks of cancer. CELL 2000;100:57–70.
17. Grivennikov SI, Greten FR, Karin M. Immunity, Inflammation, and Cancer. CELL 2010;140:883–899.
18. Greten FR, Eckmann L, Greten TF, et al. IKKbeta links inflammation and tumorigenesis in a mouse model of colitis-associated cancer. CELL 2004;118:285–296.
19. Papanikolaou A, Shank RC, Delker DA, et al. Initial levels of azoxymethane-induced DNA methyl adducts are not predictive of tumor susceptibility in inbred mice. TOXICOL APPL PHARMACOL 1998;150:196–203.
20. Bissahoyo A, Pearsall RS, Hanlon K, et al. Azoxymethane is a genetic background-dependent colorectal tumor initiator and promoter in mice: effects of dose, route, and diet. TOXICOL SCI 2005;88:340–345.
21. Maltzman T, Whittington J, Driggers L, et al. AOM-induced mouse colon tumors do not express full-length APC protein. CARCINOGENESIS 1997;18:2435–2439.
21. Takahashi M, Nakatsugi S, Sugimura T, et al. Frequent mutations of the beta-catenin gene in mouse colon tumors induced by azoxymethane. CARCINOGENESIS 2000;21:1117–1120.
23. Guillem JG, Hsieh LL, O'Toole KM, et al. Changes in expression of oncogenes and endogenous retroviral-like sequences during colon carcinogenesis. CANCER RES 1988;48:3964–3971.
24. Wang QS, Papanikolaou A, Sabourin CL, et al. Altered expression of cyclin D1 and cyclin-dependent kinase 4 in azoxymethane-induced mouse colon tumorigenesis. CARCINOGENESIS 1998;19:2001–2006.
25. Vivona AA, Shpitz B, Medline A, et al. K-ras mutations in aberrant crypt foci, adenomas and adenocarcinomas during azoxymethane-induced colon carcinogenesis. CARCINOGENESIS 1993;14:1777–1781.
26. Yabana T, Arimura Y, Tanaka H, et al. Enhancing epithelial engraftment of rat mesenchymal stem cells

restores epithelial barrier integrity. J PATHOL 2009;218:350–359.

27. Tanaka H, Arimura Y, Yabana T, et al. Myogenic lineage differentiated mesenchymal stem cells enhance recovery from dextran sulfate sodium-induced colitis in the rat. J GASTROENTEROL 2011;46:143–152.
28. Hakamata Y, Tahara K, Uchida H, et al. Green fluorescent protein-transgenic rat: a tool for organ transplantation research. BIOCHEM BIOPHYS RES COMMUN 2001;286:779–785.
29. Javazon EH, Colter DC, Schwarz EJ, et al. Rat marrow stromal cells are more sensitive to plating density and expand more rapidly from single-cell-derived colonies than human marrow stromal cells. STEM CELLS 2001;19:219–225.
30. Dominici M, Le Blanc K, Mueller I, et al. Minimal criteria for defining multipotent mesenchymal stromal cells: the International Society for Cellular Therapy position statement. CYTOTHERAPY 2006;8:315–317.
31. Goldschneider I, Gordon LK, Morris RJ. Demonstration of Thy-1 antigen on pluripotent hemopoietie stem cells in the rat. J EXP MED 1978;1441:1351–1366.
32. Kimura G, Itagaki A, Summers J. Rat cell line 3y1 and its virogenic polyoma- and sv40- transformed derivatives. INT J CANCER 1975;15:694–706.
33. Tanaka T, Kohno H, Suzuki R, et al. A novel inflammation-related mouse colon carcinogenesis model induced by azoxymethane and dextran sodium sulfate. CANCER SCI 2003;94:965–973.
34. Bird RP. Observation and quantification of aberrant crypts in the murine colon treated with a colon carcinogen: preliminary findings. CANCER LETT 1987;37:147–151.
35. McLellan EA, Bird RP. Aberrant crypts: potential preneoplastic lesions in the murine colon. CANCER RES 1988;48:6187–6192.
36. Sanger F, Nicklen S, Coulson AR. DNA sequencing with chain-terminating inhibitors. PROC NATL ACAD SCI USA 1977;12:5463-5467.
37. Sladowski D, Steer SJ, Clothier RH, et al. An improved MTT assay. IMMUNOL METHODS 1993;157:203–207.
38. Sasaki T, Yoshida K, Shimura H, et al. Inhibitory effect of linoleic acid on transformation of IEC6 intestinal cells by in vitro azoxymethane treatment. INT J CANCER 2006;118:593–599.
39. Using multivariate statistics, in: Tabachnick BG, Fidell LS, eds. Significance of group differences, 5th ed. Boston: PEASON, 2006:19–22.
40. Hu Y, Martin J, Leu RL, et al. The colonic response to genotoxic carcinogens in the rat: regulation by dietary fibre. CARCINOGENESIS 2002;23:1131–1137.
41. Takayama T, Katsuki S, Takahashi Y, et al. Aberrant crypt foci of the colon as precursors of adenoma and cancer. N ENGL J MED 1998;339:1277–1284.
42. Caderni G, Femia AP, Giannini A, et al. Identification of mucin-depleted foci in the unsectioned colon of azoxymethane-treated rats: correlation with carcinogenesis. CANCER RES 2003;63:2388–2392.
43. Le Leu RK, Brown IL, Hu Y, et al. A synbiotic combination of resistant starch and Bifidobacterium lactis facilitates apoptotic deletion of carcinogen-damaged cells in rat colon. J NUTR 2005;135:996–1001.
44. Shen L, Kondo Y, Rosner GL, et al. MGMT promoter methylation and field defect in sporadic colorectal cancer. J NATL CANCER INST 2005;97:1330–1338.
45. Sohn OS, Fiala ES, Requeijo SP, et al. Differential effects of CYP2E1 status on the metabolic activation of the colon carcinogens azoxymethane and methylazoxymethanol. CANCER RES 2001;61:8435–8440.
46. Quiros S, Roos WP, Kaina B. Processing of O^6-methylguanine into DNA double-strand breaks

requires two rounds of replication whereas apoptosis is also induced in subsequent cell cycles. CELL CYCLE 2010;9:168–178.

47. Chen J, Huang XF. The signal pathways in azoxymethane-induced colon cancer and preventive implications. CANCER BIOL THER 2009;8:1313–1317.
48. Meulmeester E, ten Dijke P. The dynamic roles of TGF-β in cancer. J PATHOL 2011;223:205–218.
49. Borinstein SC, Conerly M, Dzieciatkowski S, et al. Aberrant DNA methylation occurs in colon neoplasms arising in the azoxymethane colon cancer model. MOL CARCINOG 2010;49:94–103.
50. Kitange GJ, Mladek AC, Carlson BL, et al. Inhibition of histone deacetylation potentiates the evolution of acquired temozolomide resistance linked to MGMT upregulation in glioblastoma xenografts. CLIN CANCER RES 2012;18:4070–4079.
51. Kreth S, Limbeck E, Hinske LC, et al. In human glioblastomas transcript elongation by alternative polyadenylation and miRNA targeting is a potent mechanism of MGMT silencing. ACTA NEUROPATHOL 2013;125:671–681.
52. Labbé E, Lock L, Letamendia A, et al. Transcriptional cooperation between the transforming growth factor-beta and Wnt pathways in mammary and intestinal tumorigenesis. CANCER RES 2007;67:75–84.
53. Derynck R, Akhurst RJ, Balmain A. TGF-β signaling in tumor suppression and cancer progression. NAT GENET 2001;29:117–129.
54. Guda K, Claffey KP, Dong M, et al. Defective processing of the transforming growth factor-beta1 in azoxymethane-induced mouse colon tumors. MOL CARCINOG 2003;37:51–59.
55. Guda K, Giardina C, Nambiar P, et al. Aberrant transforming growth factor-beta signaling in azoxymethane-induced mouse colon tumors. MOL CARCINOG 2001; 31:204–213.
56. Wang QS, Guda K, Papanikolaou A, et al. Expression of transforming growth factor-beta1 and its type II receptor in mouse colon tumors induced by azoxymethane. INT J ONCOL 2000;17:551–558.
57. Bird RP, Good CK. The significance of aberrant crypt foci in understanding the pathogenesis of colon cancer. TOXICOL LETT 2000;112-113:395–402.
58. Thorup I. Histomorphological and immunohistochemical characterization of colonic aberrant crypt foci in rats: relationship to growth factor expression. CARCINOGENESIS 1997;18:465–472.
59. Shao J, Sheng H, Aramandla R, et al, Coordinate regulation of cyclooxygenase-2 and TGF-β1 in replication error positive colon cancer and azoxymethane-induced rat colonic tumors. CARCINOGENESIS 1999;20:185–191.

See www.StemCells.com for supporting information available online.